

Cite this: DOI: 10.1039/c0xx00000x

www.rsc.org/xxxxxx

ARTICLE TYPE

Compressed arsenolite As_4O_6 and its helium clathrate $\text{As}_4\text{O}_6\cdot 2\text{He}$

Piotr A. Guńka,^{*a} Kamil F. Dziubek,^{b,c} Andrzej Gładysiak,^c Maciej Dranka^a, Jacek Piechota,^d Michael Hanfland,^e Andrzej Katrusiak,^c Janusz Zachara^a

Received (in XXX, XXX) Xth XXXXXXXXX 20XX, Accepted Xth XXXXXXXXX 20XX

DOI: 10.1039/b000000x

Crystal structure of arsenolite, the cubic polymorph of arsenic(III) oxide, has been determined by single crystal X-ray diffraction up to 30 GPa. The bulk of the crystal is monotonically compressed with no detectable anomalies, to 60% of the initial volume at 30 GPa. In the structure the most compressed are $\text{As}\cdots\text{As}$ contacts which contrasts with increased intramolecular $\text{As}\cdots\text{As}$ distance in the deformed molecule. The ratio between $\text{As}\cdots\text{As}$ inter- and intramolecular distances decreases from 1.47 at 0.1 MPa to 1.03 at 30 GPa. The As_4O_6 molecules are deformed to become more tetrahedron-like. Pressure above 3 GPa favours the formation of $\text{As}_4\text{O}_6\cdot 2\text{He}$ inclusion compound in the surface layer increasingly deeper with pressure. The experimental As_4O_6 crystal compression has been compared with various theoretical models within the DFT framework. According to band-structure calculations the arsenolite band gap falls from 4.2 eV at ambient pressure to 2.7 eV at 27.8 GPa.

Introduction

Arsenolite is a well-known mineral till recently generally used for various industrial, agricultural, chemical and household applications owing to its strong toxicity and exceptional properties. Polymorphism of arsenic(III) oxide has attracted attention for years. There are two minerals of As_2O_3 – cubic arsenolite containing adamantane-like As_4O_6 molecules packed in a 3D diamond network^{1,2} and monoclinic claudetite I consisting of highly corrugated As_2O_3 layers^{3–5}. In the late 1940s another monoclinic modification was discovered and called claudetite II due to its extended As_2O_3 layers resembling those of claudetite I.^{6,7} Well-known is also a glassy As_2O_3 modification. There are a few reports on the studies of arsenic(III) oxide polymorphs under high pressure. The arsenolite-claudetite I equilibrium as a function of temperature and pressure was studied extensively in the 1960s. It was suggested that arsenolite undergoes a reversible transition to claudetite I at $110\pm 10^\circ\text{C}$ when subjected to shear stress.⁸ In another high-pressure (HP) study of arsenolite, claudetite I and glassy As_2O_3 , Soignard *et al.* compressed arsenolite in non-hydrostatic conditions up to 35 GPa and observed its amorphisation above 20 GPa.⁹ Grzechnik's Raman and IR spectroscopy study of arsenolite up to 16 GPa suggested a phase transition at 6 GPa, lowering the cubic symmetry to tetragonal and retaining two molecules per the primitive unit cell. He also noted that hydrostatic or quasi-hydrostatic pressure, as opposed to shear stress, does not induce arsenolite-claudetite I transition.¹⁰ However, no structural information about the HP arsenolite and its compressibility was measured. Presently we report this information determined by synchrotron single-crystal X-ray diffraction up to 30 GPa and theoretically modelled by DFT calculations. They reveal considerable structural transformations reducing the molecular character of the crystal, supported by DFT band structure and

density of states for arsenolite at ambient pressure and around 30 GPa. We also found a pressure-induced solvation of arsenolite with helium above 3 GPa.

Results and discussion

Crystal structure and diffraction pattern

At ambient pressure arsenolite is a typical molecular crystal. It is built of adamantanoid As_4O_6 molecules (Fig. 1) located at highly symmetric $4\bar{3}m$ sites of cubic space group $Fd\bar{3}m$. The bulk of the crystal is monotonically compressed in the whole pressure range of our study. No anomalies have been detected to 30 GPa either in the lattice parameters (Fig. 2) or in the intermolecular distances and molecular dimensions (Figs. 3 and 4). This indicates that previously observed anomalies at 6 GPa in the Raman and IR spectra of mixed arsenolite and CsI powders¹⁰ were caused by the non-hydrostatic effects in the sample, rather than any phase transition in arsenolite. In our study He environment ensured perfectly hydrostatic conditions to 11.6 GPa, and pseudo-hydrostatic conditions above,¹¹ whereas CsI is harder than arsenolite even at normal conditions.

Pressure induces systematic distortions of the molecular geometry (Figs. 3 and 4). Although no changes in the $\text{As}-\text{O}$ bond length can be noted within experimental error, $\text{As}-\text{O}-\text{As}$ and $\text{O}-\text{As}-\text{O}$ bond angles are bent in the opposite sense and consequently, the intramolecular distances $\text{As}\cdots\text{As}$ increase and $\text{O}\cdots\text{O}$ decrease (Fig. 3). These changes, of about 2% of the ambient-pressure values, are much smaller than the compression of intermolecular contacts. Oxygen atoms are pushed towards $\text{As}\cdots\text{As}$ intramolecular edges which are elongated as pressure increases and the molecule becomes more tetrahedron-like. This is most likely the result of the $\text{O}\cdots\text{O}$ packing interactions which have already been found to be very important in the understanding of silicate structures under

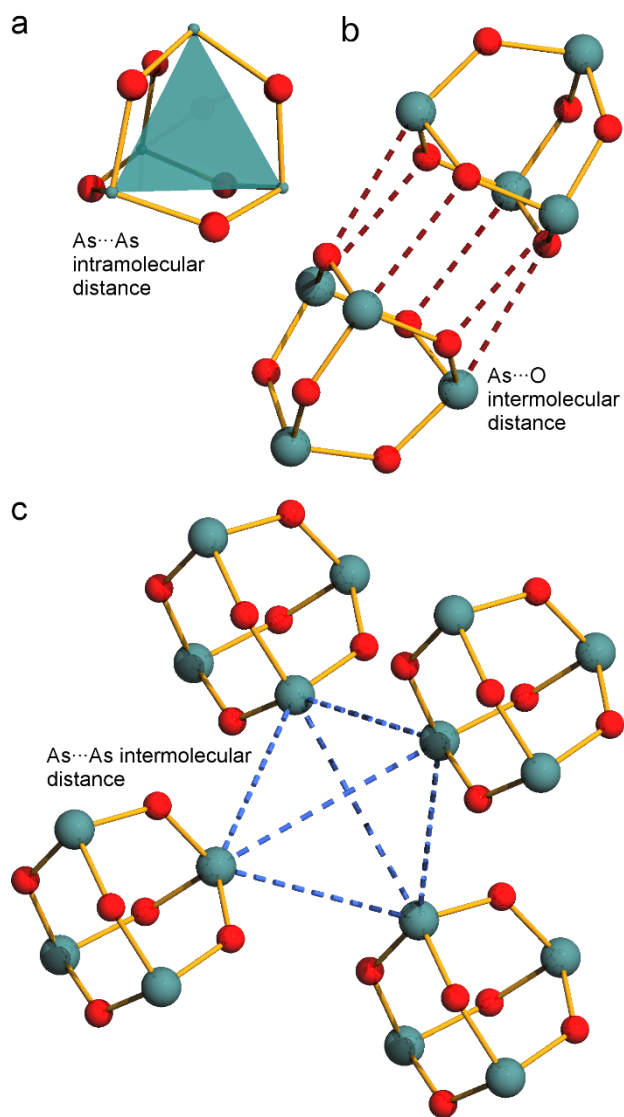


Fig. 1 (a) Molecular structure of arsenolite with As_4 tetrahedron marked in green; (b) $(\text{As}_4\text{O}_6)_2$ dimer with $\text{As}\cdots\text{O}$ separations marked with dashed brown lines; (c) $(\text{As}_4\text{O}_6)_4$ cluster with $\text{As}\cdots\text{As}$ intermolecular distances marked with light blue dashed lines.

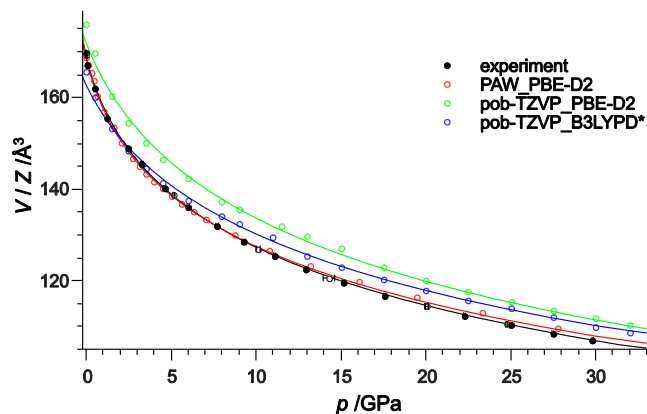


Fig. 2 EoS curves for experimental and theoretical ($p, V/Z$) data. Filled and empty black circles denote experimental data corresponding to compression and decompression, respectively.

below the level of As and O van der Waals radii sum (3.37 \AA^{13}) and they fall steadily upon pressure increase. The $\text{As}\cdots\text{As}$ separation in the tetrahedral $(\text{As}_4\text{O}_6)_4$ clusters decreases from $4.6090(5) \text{ \AA}$ at 0.1 MPa to $3.4268(7) \text{ \AA}$ at 30 GPa , passing the 15 doubled As van der Waals radius (3.70 \AA) at 15 GPa . The $\text{As}\cdots\text{As}$ distance at 30 GPa equals 74% of that at ambient pressure, while the analogous ratio for the $\text{As}\cdots\text{O}$ contact at 30 GPa is 79%, indicating that the compression of tetrahedral clusters is slightly more significant than the compression of As_4O_6 dimers (see Fig. 20 1b,c).

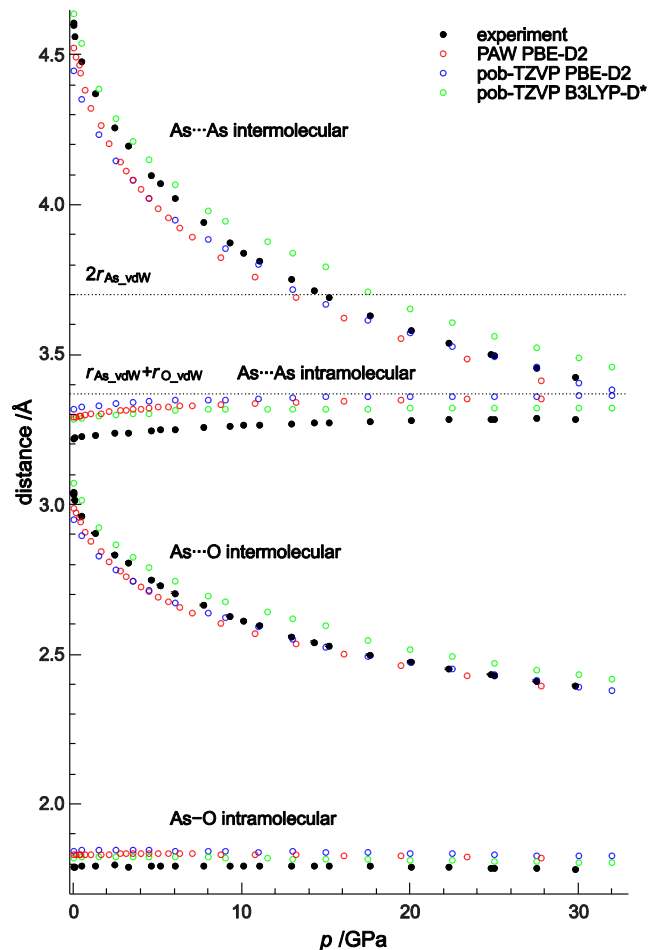


Fig. 3 As-O bond length, intramolecular $\text{As}\cdots\text{As}$ separation as well as intermolecular $\text{As}\cdots\text{O}$ and $\text{As}\cdots\text{As}$ distances plotted as a function of pressure for both experimental and theoretical data.

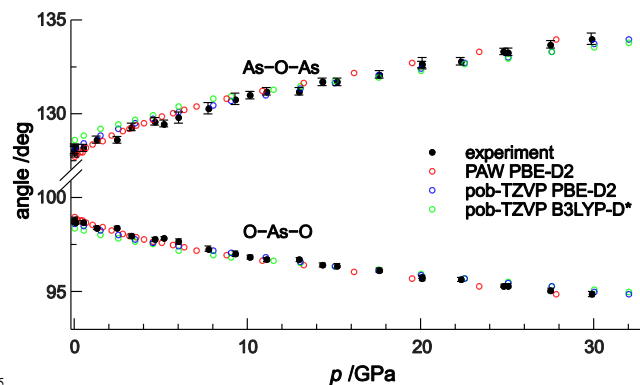


Fig. 4 O-As-O and As-O-As bond angles plotted as a function of pressure for both experimental and theoretical data.

10 high pressure.¹² The intermolecular $\text{As}\cdots\text{O}$ distances are all well

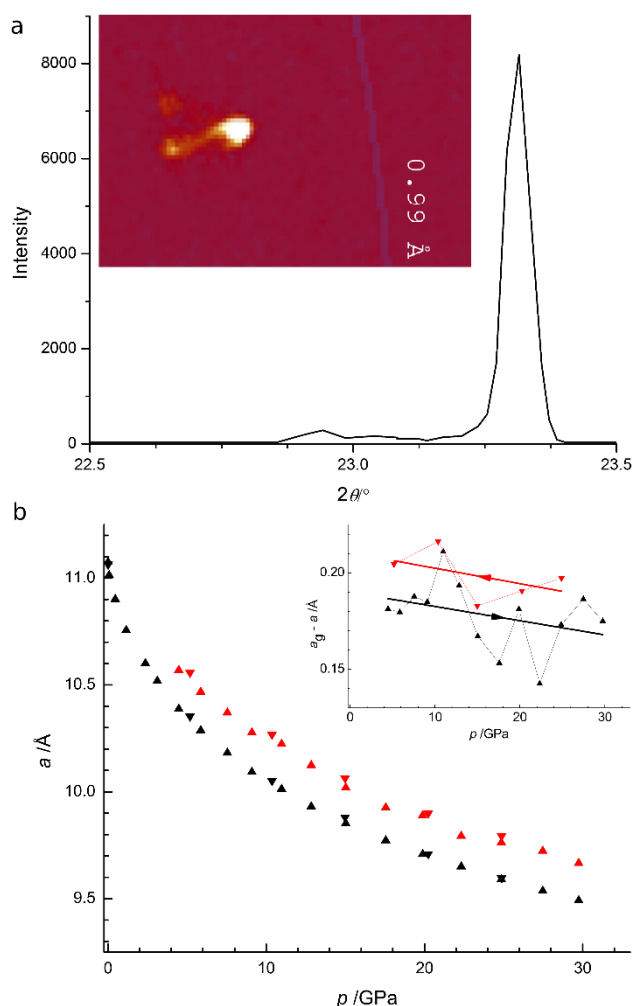


Fig. 5 (a) Reflection $\bar{4}8\bar{4}$ profile, extended to include the “ghost” reflection of the arsenolite–helium inclusion compound. The Bragg–“ghost” reflections pair recorded in the diffraction image is also shown in the inset (the blue line corresponds to the resolution of $d = 0.99 \text{ \AA}$). (b) Lattice parameter a of arsenolite (black symbols) and a_g of the lattice formed by the “ghost” reflections (red symbols). Triangles up stand for compression, triangles down – decompression. In the inset difference between the lattice parameter a and a_g is plotted against pressure. Black symbols correspond to the compressed sample, whereas red ones – to its decompression.

Starting from 3.28(9) GPa additional weak “ghost” reflections appear on the lower 2 θ -angle side of the main reflections of the As_4O_6 sample (see Figs. 5a and S1). The intensity of most of these “ghost” reflections increases with pressure, reaching 10–15% of the main reflections at the 29.83(5) GPa limit of our data (see Fig. S2). The “ghost” reflections can be indexed according to the face-centered cubic lattice with the parameter a_g being about 2% longer than that of the main As_4O_6 crystal. This ratio is somewhat smaller for the series of measurements with the compressed sample than for the decompression run (Fig. 5b and Table S5). After eliminating possibilities of instrumental artefacts, of spurious radiation or multiple diffraction as the origin of the “ghost” reflections, they have been associated with the formation of $\text{As}_4\text{O}_6 \cdot 2\text{He}$ inclusion compound promoted by pressure higher than 3.28(9) GPa.

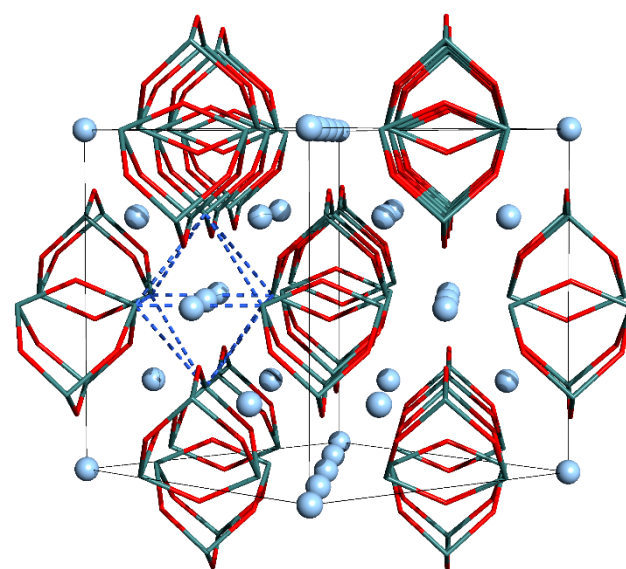


Fig. 6 Crystal structure of $\text{As}_4\text{O}_6 \cdot 2\text{He}$ inclusion compound viewed along $\sim[110]$. As_4O_6 molecules are represented in wireframe model, whereas He atoms as light-blue balls. Dashed blue lines indicate deformed octahedral surrounding of He by arsenic atoms (see Fig. S3 for a closer view).

This compound is formed on the surface of arsenolite sample and the He-permeation depth increases with pressure, as indicated by the intensity of “ghost” reflections. The formation and decomposition of the $\text{As}_4\text{O}_6 \cdot 2\text{He}$ clathrate have been supported by a small hysteresis of “ghost”-lattice unit-cell volume upon sample compression and decompression (Fig. 5b). The diffusion of “ghost” reflections can be due to the strain between the crystal bulk and the helium-permeated surface. When assuming the helium atom position in the largest voids, located at 0, 0, 0 (Fig. 6), an improved fit between observed and calculated structure factors has been obtained. Although the precise read-out of the intensity of “ghost” reflections is hampered by their diffusion and proximity of much stronger main reflections, the simple structure of $\text{As}_4\text{O}_6 \cdot 2\text{He}$ allows the determination of intermolecular distances in this crystal. The closest $\text{As} \cdots \text{He}$ contact is 2.7456(18) \AA at 7.71(8) GPa and 2.4517(14) \AA at 29.83(5) GPa, whereas the closest $\text{O} \cdots \text{He}$ contacts are 2.698(11) \AA and 2.444(4) \AA , respectively. These distances are compatible with van der Waals radii of helium, arsenic and oxygen when taking into account their considerable compression in this pressure range. Further investigations in different pressure transmitting media are planned to verify the hypothesis.

Recently, a high-pressure structural study on senarmontite – cubic antimony(III) oxide has been carried out. It undergoes two isostructural phase transitions at 3.5 and 10 GPa consisting in adamantane-like Sb_4O_6 molecules becoming 3D covalent network. Cubic symmetry has been retained during the transitions but significant changes in bulk modulus have occurred.¹⁴ Similar effects were not observed for arsenolite up to 30 GPa and this could be related to the fact that intermolecular contacts in senarmontite are shorter than in arsenolite at ambient pressure as evidenced by the $\text{Sb} \cdots \text{O}$ and $\text{As} \cdots \text{O}$ contacts of 2.9018(9) and 3.041(2) \AA , respectively.¹⁵ Interestingly, the geometry of As_4O_6 molecule under 20.07(9) GPa is very similar to that of Sb_4O_6 at ambient pressure, as evidenced by the bond angles and bond valency values (see Table S6). This suggests that the crystal structure of senarmontite at a given pressure is very similar to that of arsenolite

but under higher pressures. It could be concluded then that arsenolite should undergo isostructural transitions similar to that observed in senarmontite under pressures higher than 30 GPa.

Crystal structure – comparison between experiment and computations

We performed theoretical calculations of arsenolite crystal structure under pressure utilising various quantum mechanical models to compare their accuracy in the description of the system. We utilised density functional theory (DFT)^{16,17} with two various basis sets – plane waves and localised Gaussian type atomic orbitals in the form of pob-TZVP basis set¹⁸. Two functionals with dispersion corrections treated with the Grimme method were studied, namely PBE-D2 functional from the GGA family of functionals^{19,20} and the hybrid B3LYP-D* functional with the Grimme correction optimised for solid state calculations by Civalleri *et al*²¹. A total of three models denoted PAW_PBE-D2, pob-TZVP_PBE-D2 and pob-TZVP_B3LYP-D* were tested. The PAW calculations performed with the VASP code were carried out as constant volume optimisations and the external pressure was the result of the volume constraint whereas the pob-TZVP computations, effected in the CRYSTAL09 suite, were executed as full geometry optimisations under external pressure defined in the input. Interestingly, all of the models overestimate the As–O bond lengths by ca. 0.03-0.05 Å (*cf.* Fig. 2). The discrepancies for As⋯O intermolecular distances are a little smaller and the PBE-D2 model has been found to perform better than the B3LYP-D*. The agreement between experimental and calculated As–O–As and O–As–O bond angles is remarkable with most of the calculated values lying within one standard uncertainty (s.u.) from the experimental values.

Equation of state

Third order Birch-Murnaghan equation of state (EoS):²²

$$p = \frac{3B_0}{2} \left(\left(\frac{V_0}{V} \right)^{\frac{7}{3}} - \left(\frac{V_0}{V} \right)^{\frac{5}{3}} \right) \left[1 + \frac{3}{4} (B'_0 - 4) \left(\left(\frac{V_0}{V} \right)^{\frac{2}{3}} - 1 \right) \right]$$

where V_0 is volume at zero pressure, B_0 bulks modulus and B'_0 is bulk modulus first derivative with respect to pressure, has been fitted to the experimental as well as theoretical ($p, V/Z$) set of points using weights for both pressure and volume s.u.'s. Z is the number of As_4O_6 molecules in the unit cell and consequently V/Z is molecular volume. The resulting EoSs parameters are given in the Table 1 and the EOSs curves are plotted together with experimental and computed points in Fig. 2.

Table 1 Third-order Birch-Murnaghan EoS parameters for experimental and computational set of ($p, V/Z$) points.

	V_0/Z^3 Å ³	B_0 / GPa	B'_0
experiment	168.7(6)	11.8(5)	8.6(2)
PAW_PBE-D2	169.1(4)	10.0(5)	10.5(4)
pob-TZVP_PBE-D2	162.8(14)	21(2)	7.0(5)
pob-TZVP_B3LYPD*	172.0(18)	18(2)	6.4(5)

^a V_0/Z is molecular volume at zero pressure

Agreement between the experimental and PAW_PBE-D2 data is extraordinary. It is noteworthy that these calculations were performed in the $P1$ space group and the analysis of the optimised geometries indicates that they all exhibit the symmetry of the cubic

$Fd\bar{3}m$ space group which supports our experimental result that no lowering of symmetry occurs in arsenolite upon compression. Surprisingly, the agreement is worst for the pob-TZVP_B3LYP-D* model even though the B3LYP functional is used extensively for computations of molecules and the dispersion correction has been optimised for molecular crystals. The application of Gaussian basis set leads to significant overestimation of the bulk modulus and also to significant increase in its standard uncertainty.

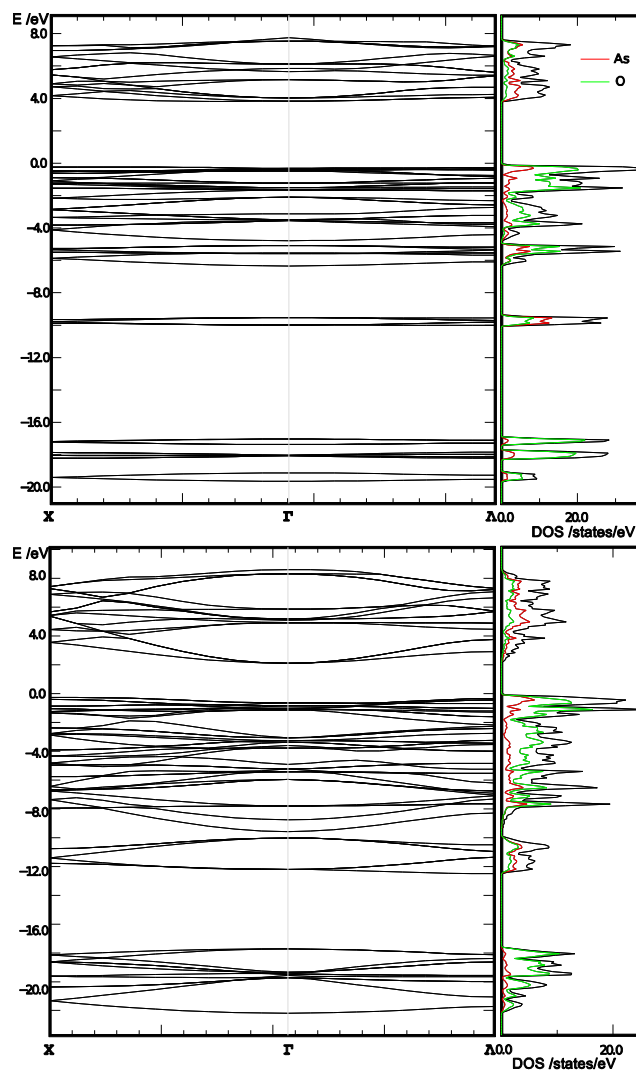


Fig. 7 Band structure and density of states (DOS) in arsenolite crystal structures at 0.06 GPa (top) and at 27.8 GPa (bottom). Red and green lines denote As and O partial DOS, respectively. X stands for (0.5, 0.5, 0), Γ for (0, 0, 0) and Λ for (0.5, 0.5, 0.5) points in the reciprocal lattice.

Band structure

Band structure and density of states (DOS) have been computed to see if any interesting changes occur in the arsenolite's electronic structure upon compression, given that As⋯As separations fall below the sum of As van der Waals radii as pressure increases (see Fig. 3). PAW method with plane wave basis set was utilised with PBE exchange-correlation functional and Grimme's D2 correction for dispersion. Computations have shown that arsenolite is an insulator at 0.06 GPa with a band gap of 4.2 eV which drops to 2.7 eV making cubic As_2O_3 semiconducting at 27.8 GPa (Fig. 7).

Electronic bands tend to be more diffuse at high pressure, but no significant changes in the As and O partial DOS relative to one another have occurred upon the pressure increase.

Conclusions

The arsenolite crystal structure in the pressure range from 0 to 30 GPa is compressed monotonically and no phase transitions have been detected. The crystal structure undergoes smooth compression and decompression without hysteresis in the studied pressure range. The As atoms are displaced toward outside of As₄O₆ molecules with pressure and O atoms are simultaneously pushed inside which makes the molecule more tetrahedron-like. The compression affects the As...As intermolecular distances more than As...O separations, which at 30 GPa amount to 74% and 79% of the ambient-pressure values, respectively. The experimentally measured effects compare well with different quantum mechanical models. None of the calculations pointed to a phase transition either. It has been found that plane wave basis set and PBE functional augmented with the Grimme's dispersion correction (PBE-D2) yield the best predictions and the application of the pob-TZVP Gaussian basis set leads to the overestimation of arsenolite bulk modulus. The computations of arsenolite band structure indicate that its band gap decreases from 4.2 eV at ambient pressure to 2.7 eV at 27.8 GPa. Last but not least, we have found very convincing experimental evidence of the formation of As₄O₆·2He inclusion compound whose crystal structure is proposed. To the best of our knowledge this is the first report on a noble gas inclusion compound in a host lattice of a molecular oxide.

Acknowledgements

This work has been supported by the National Science Centre, grant no. DEC-2012/05/N/ST5/00283. K.F.D. gratefully acknowledges the Polish Ministry of Science and Higher Education for financial support through the "Mobilność Plus" program. The VASP calculations were carried out in the Interdisciplinary Centre for Mathematical and Computational Modelling (computational grant No. G28-3), whereas the CRYSTAL09 computations were performed using resources provided by the Wrocław Centre for Networking and Supercomputing (<http://wcss.pl>), grant no. 260. We acknowledge the European Synchrotron Radiation Facility for provision of synchrotron radiation facilities.

Notes and references

a Warsaw University of Technology, Faculty of Chemistry, Noakowskiego 3, 00-664 Warszawa, Poland, e-mail:

a piogun@ch.pw.edu.pl

b LENS, European Laboratory for Non-Linear Spectroscopy, Via Nello Carrara 1, 50019 Sesto Fiorentino, Italy

c Faculty of Chemistry, Adam Mickiewicz University, Umultowska 89b, 61-614 Poznań, Poland

d Interdisciplinary Centre for Mathematical and Computational Modelling, University of Warsaw, Pawińskiego 5a, 02-106 Warsaw, Poland

e ESRF, 6 rue Jules Horowitz, BP 220, F-38043 Grenoble Cedex, France

† Electronic Supplementary Information (ESI) available: experimental and computational details, cif files with experimental structures,

experimental and theoretical structural parameters. See DOI: 10.1039/b000000x/

References

- 1 R. M. Bozorth, *J. Am. Chem. Soc.*, 1923, **45**, 1621–1627.
- 2 F. Pertlik, *Czech. J. Phys.*, 1978, **28**, 170–176.
- 3 K. A. Becker, K. Plieth and I. N. Stranski, *Z. Anorg. Allg. Chem.*, 1951, **266**, 293–301.
- 4 A. J. Frueh, *Am. Mineral.*, 1951, **36**, 833–850.
- 5 F. Pertlik, *Monatsh. Chem.*, 1978, **109**, 277–282.
- 6 E. Kürbs, K. Plieth and I. N. Stranski, *Z. Anorg. Chem.*, 1949, **258**, 238–246.
- 7 F. Pertlik, *Monatsh. Chem.*, 1975, **106**, 755–762.
- 8 W. B. White, F. Datchile and R. Roy, *Z. Kristallogr.*, 1967, **125**, 450–458.
- 9 E. Soignard, S. A. Amin, Q. Mei, C. J. Benmore and J. L. Yarger, *Phys. Rev. B*, 2008, **77**, 144113.
- 10 A. Grzechnik, *J. Solid State Chem.*, 1999, **144**, 416–422.
- 11 K. Takemura, *High Pressure Research*, 2007, **27**, 465–472.
- 12 C. T. Prewitt and R. T. Downs, in *Ultra-high-pressure mineralogy: physics and chemistry of the earth's deep interior*, Mineralogical Society of America, Washington, DC, 1998, pp. 283–317.
- 13 A. Bondi, *J. Phys. Chem.*, 1964, **68**, 441–451.
- 14 A. L. J. Pereira, L. Gracia, D. Santamaría-Pérez, R. Vilaplana, F. J. Manjón, D. Errandonea, M. Nalin and A. Beltrán, *Phys. Rev. B*, 2012, **85**, 174108.
- 15 A. E. Whitten, B. Dittrich, M. A. Spackman, P. Turner and T. C. Brown, *Dalton T.*, 2004, 23–29.
- 16 P. Hohenberg and W. Kohn, *Phys. Rev.*, 1964, **136**, B864–B871.
- 17 W. Kohn and L. J. Sham, *Phys. Rev.*, 1965, **140**, A1133–A1138.
- 18 M. F. Peintinger, D. V. Oliveira and T. Bredow, *J. Comput. Chem.*, 2013, **34**, 451–459.
- 19 J. P. Perdew, K. Burke and M. Ernzerhof, *Phys. Rev. Lett.*, 1996, **77**, 3865–3868.
- 20 J. P. Perdew, K. Burke and M. Ernzerhof, *Phys. Rev. Lett.*, 1997, **78**, 1396.
- 21 B. Civalleri, C. M. Zicovich-Wilson, L. Valenzano and P. Ugliengo, *CrystEngComm*, 2008, **10**, 405–410.
- 22 F. Birch, *Phys. Rev.*, 1947, **71**, 809–824.